Intracochlear Motion Measurement in the Basal Turn of the Guinea Pig Cochlea: A Comparison Across Species and Cochlear Locations

[1]Lauren Chiriboga, [2]C. Elliott Strimbu, [3]Brian Frost, [1,2]Elizabeth S. Olson

[1] Department of Biomedical Engineering Columbia University, New York City, NY
[2] Department of Otolaryngology-Head & Neck Surgery, Columbia University, New York City, NY
[3] Department of Electrical Engineering, Columbia University, New York City, NY

Corresponding author email: lauren.chiriboga@columbia.edu

T50

Introduction

Optical coherence tomography (OCT) has become a primary means for collecting sub-nanometer vibration data throughout the organ of Corti complex (OCC). While gerbils and mice are the cochlear mechanics community's primary animal models, guinea pigs can provide further insight into cochlear micromechanics and another set of conditions for which models should comply [1].

Using OCT, we image and measure the motion of the first turn of the guinea pig cochlea through the round window membrane (RWM) and a cochleostomy at various optical angles relative to the tissue.

Cooper et al. have characterized an area of large activity extending throughout the OCC near the outer hair cells (OHCs) in gerbil, deemed the "hotspot" [2]. Gerbils have been found to have extensive sub-best frequency (BF) activity, which is heightened when presented with multi-tone stimuli [3-4]. However, this observation is rare in guinea pigs and difficult to replicate. Here, we further explore and compare different trends in intra-OCC motion in guinea pig and gerbil.

Methods

- ❖ 1300 nm spectral domain OCT was used for imaging and vibrometry, as described previously [5]
- ❖ Multi-tone Zwuis stimuli were used, containing 35 stimulus frequencies between 5-40 kHz [6]
- ❖ Noise is defined as the average of the 5 neighboring points on either side of each frequency in the stimulus
- ❖ Data is considered sufficiently out of the noise when motion was > 2.5 times the SD of the noise
- ❖ Motion measurements and imaging were conducted through the RWM, followed by a cochleostomy in the first turn
- ❖ Hearing health was monitored by DPOAE measurements before and after cochleostomy
- ❖ Optical and anatomical coordinates registered as described in [7]

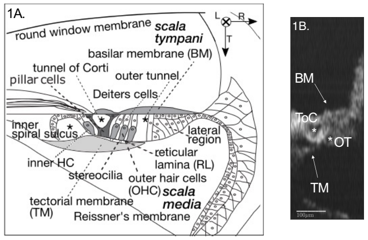

Figure 1: A: Simplified rendering of a radial-transverse cross-section of the organ of Corti in the gerbil cochlear base. Structures of interest are the Basilar Membrane (BM), Tectorial Membrane (TM), outer hair cells (OHCs), reticular lamina (RL), stereocilia, scala media (SM), scala tympani (ST). B: OCT Bscan of the radial-transverse cross-section with some structures of interest identified.

Figure 2: Image of a cochleostomy conducted in GP69. Cochleostomies were performed in the first turn of the guinea pig cochlea. Hearing health was assessed before and after via DPOAEs. ST is the first accessed space through both the RW and cochleostomy, with the BM as the visible component of the OCC.

Figure 3: Distortion product otoacoustic emissions (DPOAEs) at 50 (top) and 70 (bottom) dB sound pressure level (SPL), from the experiments presented. Dashed lines represent noise levels.

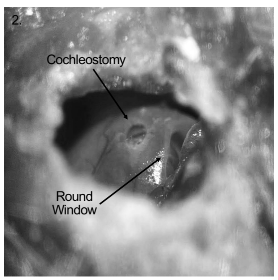

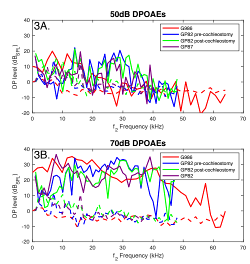

Results

Guinea Pig RWM – transverse view

- ❖ Sub-BF nonlinearity refers to sub-BF frequencies having increasing gain as stimulus pressure decreases across most/all sub-BF frequencies.
- ❖ Some measurements through the RWM contain small areas of sub-BF nonlinearity near the OHCs apex/stereocilia/reticular lamina region (RL).
- ❖ Phase shifts up to ¼ cycle re: BM are seen in the sub-BF region but become in phase with BM closer to BF.

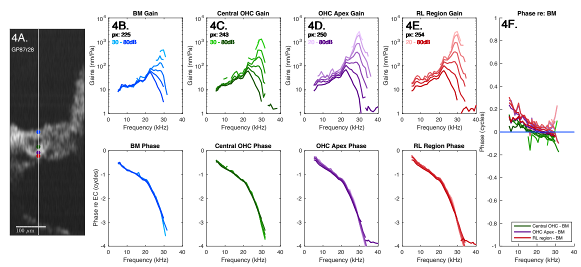

Figure 4: GP87 run 28 - Bscan, gain, and phase data through the RWM in the guinea pig cochlea. A: Bscan corresponding to run 28 vibrometry data. White line indicates the central axis of Ascan, along which vibrometry data was taken. Y-axis is scaled by 2.7 μm per pixel. Colored dots indicate locations in depth from which vibrometry data were taken. B-E: Gain in nm/Pa (top) and phase re: ear canal in cycles (bottom) from the BM (B), central OHC (C), OHC apex (D), and RL region (F). Labels for each point are estimates of the structure based on the Bscan. OHC apex and RL region responses contain sub-BF nonlinearity but not activity. F: BM phase subtracted from that of each structure. Phases start ¼ cycle out of phase with BM and sub-BF frequencies, then meet the BM phase near the BF. Longitudinal, radial, and transverse components (l, r, t) of motion are obtained by registration with optical coordinates as described in Frost et al. 2022. (l, r, t) = (0.2, -0.3, 0.9)

Guinea Pig RWM and Cochleostomy

- ❖ Some data through RWM contain no substantial sub-BF nonlinearity; OHC apex/RL region act like BM.
- ❖ Enhanced gain across all frequencies sometimes appears through the cochleostomy at the central OHC pixels along with a sustained/increasing phase lag, except for 80dB SPL, in which the phase begins to lift near BF.

GP82 through RWM

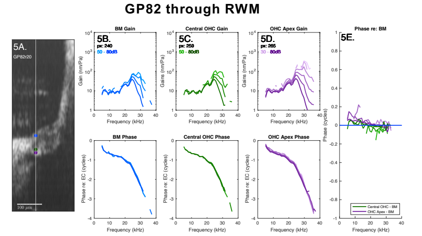

Figure 5: GP82 run 20 – Bscan, gain, and phase data through the RWM of the guinea pig cochlea. A: Bscan of the OCC. B-D: Gain in nm/Pa (top) and phase re: ear canal in cycles (bottom) from the BM (B), central OHC (C), and OHC apex (D). Labels for each point are estimates of the structure based on the Bscan. E: Phase of Central OHC and OHC apex minus BM. The horizontal line at 0 represents BM. The structures remain in phase with BM across frequencies, contrasting with instances with sub-BF activity in which there are phase differences.

GP82 through cochleostomy

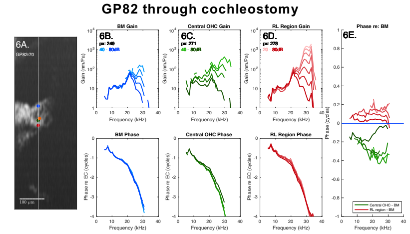

Figure 6: GP82 run 70 – Bscan, gain, and phase data obtained through a cochleostomy in the first turn of the guinea pig cochlea. A: Bscan of the OCC through the cochleostomy. The lateral side of the OCC is obstructed by one of the walls of the cochleostomy. The cochleostomy was not expanded to prevent damage. B-D: Gain and phase data from the BM (B), central OHC (C), and RL region (D). Labels for each point are estimates of the structure based on the Bscan. F: Phase of central OHC, neighbor OHC, and RL region minus BM. The horizontal line at 0 represents BM. While the RL region appears to remain approximately in phase with BM, the OHC apex point has a persistent phase lag across frequencies, except at 80 dB, which lifts as the frequency approaches BF. (l, r, t) – (-0.5, -0.1, 0.9)

Gerbil RWM

- ❖ OHC data from the gerbil RWM has been shown to contain both enhanced gain across frequencies and sub-BF nonlinearity, resembling GP cochleostomy data (fig. 6).

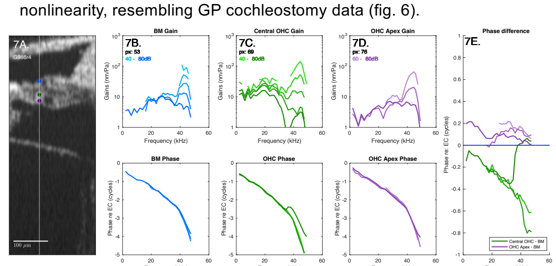

Figure 7: G986 run 4 [8] - Bscan, gain, and phase data through the RWM in the gerbil cochlea. A. Bscan corresponds to the run 4 vibrometry data. B-D: Gain in nm/Pa (top) and phase re: ear canal in cycles (bottom) from the BM (B), central OHC (C), and OHC apex (D). The central OHC sub-BF gain has a large amount of activity and nonlinearity. These traits are not seen in the BM or OHC apex data. E: BM phase was subtracted from central OHC and OHC apex phases. The central OHC point is comparable to BM phase at low frequencies, increasing in phase difference as the BF is approached, except for 80dB, which lifts to be in phase with BM near BF. OHC apex remains relatively constant at a ¼ cycle lead re: BM. (l, r, t) = (-0.48, -0.35, 0.8)

Discussion

- ❖ Internal OHC motion was obtained by taking the vector difference (VD) of measured OHC motion – BM motion
- ❖ Behavior of measured vs. internal OHC motion re: BM is different in the different instances of sub-BF activity/nonlinearity (GP87 vs. GP82)

GP87r28 Vector Difference through RWM

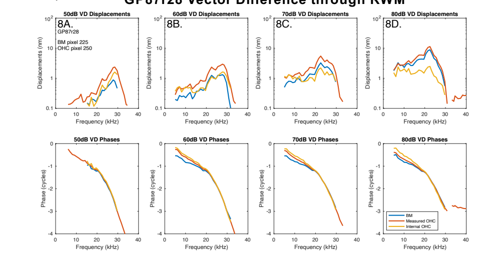

GP82r70 Vector Difference through cochleostomy

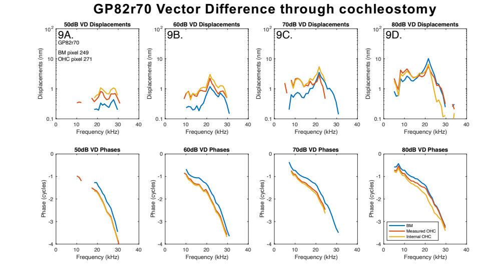

Figure 8: Vector difference magnitude (A-D top) and phase (A-D bottom) from GP87 run 28 BM and OHC apex. The blue line is BM, the red line is measured OHC, and the yellow line is internal OHC, taken by vector subtracting measured OHC-BM.

Figure 9: Vector difference magnitude (A-D top) and phase (A-D bottom) from GP82 run 70 BM and central OHC (A-D).

Conclusions

The guinea pig base sometimes exhibits distinctive behavior, including sub-BF nonlinearity and/or enhanced gain. Further, this behavior most frequently presents near the OHC apex/RL region. However, this result is not consistently repeatable, as there are instances where no sub-BF nonlinearity or gain increase is present.

Even with similar transverse components, the behaviors appear different between measurements through the RWM as opposed to through a cochleostomy in some preparations. These differences include nonlinearity and heightened gain at sub-BF frequencies and appearing in regions more central in the OCC through the cochleostomy.

Vector differences provide a more nuanced perspective to intra-OCC motions re: BM across frequencies, illuminating destructive interference between different structures, their contributions to the overall motion of the OCC, and how those contributions change with stimulus amplitude.

References

[1] E. Fallah, C. E. Strimbu, and E. S. Olson, "Nonlinearity of intracochlear motion and local cochlear microphonic: Comparison between guinea pig and gerbil," *Hearing Research*, vol. 405, p. 108234, Jun. 2021, doi: 10.1016/j.heares.2021.108234.

[2] N. P. Cooper, A. Vavakou, and M. van der Heijden, "Vibration hotspots reveal longitudinal funneling of sound-evoked motion in the mammalian cochlea," *Nat Commun*, vol. 9, p. 3054, Aug. 2018, doi: 10.1038/s41467-018-05483-z.

[3] E. Fallah, C. E. Strimbu, and E. S. Olson, "Nonlinearity and amplification in cochlear responses to single and multi-tone stimuli," Hearing Research, vol. 377, pp. 271–281, Jun. 2019, doi: 10.1016/j.heares.2019.04.001.

[4] C. P. C. Versteegh and M. van der Heijden, "Basilar Membrane Responses to Tones and Tone Complexes: Nonlinear Effects of Stimulus Intensity," JARO, vol. 13, no. 6, pp. 785–798, Dec. 2012, doi: 10.1007/s10162-012-0345-0.

[5] C. E. Strimbu, Y. Wang, and E. S. Olson, "Manipulation of the Endocochlear Potential Reveals Two Distinct Types of Cochlear Nonlinearity," Biophysical Journal, vol. 119, no. 10, pp. 2087–2101, Nov. 2020, doi: 10.1016/j.bpj.2020.10.005.

[6] M. van der Heijden and P. X. Joris, "Cochlear Phase and Amplitude Retrieved from the Auditory Nerve at Arbitrary Frequencies," *J Neurosci*, vol. 23, no. 27, pp. 9194–9198, Oct. 2003, doi: 10.1523/JNEUROSCI.23-27-09194.2003.

[7] B. L. Frost, C. E. Strimbu, and E. S. Olson, "Using volumetric optical coherence tomography to achieve spatially resolved organ of Corti vibration measurements," *The Journal of the Acoustical Society of America*, vol. 151, no. 2, pp. 1115–1124, Feb. 2022, doi: 10.1121/10.0009576.

[8] C. E. Strimbu, L. A. Chiriboga, B. L. Frost, and E. S. Olson, "Regional differences in cochlear nonlinearity across the basal organ of Corti of gerbil," *Hearing Research*, p. 108951, Jan. 2024, doi: 10.1016/j.heares.2024.108951.

Acknowledgements

This work is supported by the NIDCD and the Emil Capita Foundation. We thank Kaitlyn Wong, Sharon Feng, Nicolas Waring, and Arielle Joasil for their valuable input and support.